

Temporal stability analysis of high Mach number boundary layers over cooled impedance walls

By L. De Broeck,[†] S. Görtz,^{†‡} T. Flint, C. Gonzalez, M. Oberlack^{†‡} AND S. Lele

The temporal linear stability of a high Mach number exponential boundary layer flow over a highly cooled impedance wall is investigated, considering both the inviscid and viscous cases. For the inviscid linear stability equations an exact solution is derived, allowing the stability problem to be reduced to an algebraic eigenvalue equation. The inviscid eigenvalues and eigenfunctions are compared to those obtained for the viscous equations computed using a spectral Chebyshev collocation method. Good agreement between both results is observed in terms of the dominant and discrete modes. The analysis reveals that the dominant mode has an inviscid origin. Furthermore, the combined effects of wall impedance and its temperature on the dominant second mode are examined. Here, both the inviscid and viscous results reveal that wall impedance has a damping effect on the second mode, while increasing wall cooling leads to further destabilization.

1. Introduction

Since drag and surface heating are considerably higher in turbulent boundary layer flows than in laminar ones, understanding and predicting the laminar-turbulent transition of boundary layers are essential for many technical applications. An example is the design of hypersonic vehicles, where the increased aero-thermal load due to transition of the hypersonic boundary layer from laminar to turbulent requires stronger thermal protection systems of the vehicle, leading to a higher vehicular weight at the expense of maximum payload and flight performance (Fievet et al. 2020). However, a reliable prediction of the transition from laminar to turbulent is still challenging, making conservative vehicle design with the consequence of higher weight necessary (Bitter & Shepherd 2015). Therefore, investigations of hypersonic boundary layer transition are of key practical importance for gaining a better understanding of the occurrence of transition and taking mitigation measures.

In a low-disturbance environment, the cause of the transition of a flow from laminar to turbulent is the growth of unstable disturbances (Fedorov 2011). Since the pioneering work of Lees & Lin (1946) based on an asymptotic analysis of the boundary layer stability problem, numerous numerical and experimental studies have been carried out to shed light on the stability behavior of supersonic and hypersonic boundary layer flows. A decisive contribution to the understanding of compressible boundary layer stability was achieved by the numerical work of Mack (1969, 1984) employing linear stability theory. He confirmed the findings of Dunn & Lin (1955) that in compressible boundary layers at moderate supersonic Mach numbers, instabilities can arise through unstable mechanisms and are analogous to the well-known Tollmien-Schlichting waves. Here, the

[†] Fluid Dynamics, TU Darmstadt, Germany

[‡] Graduate School of Computational Engineering, TU Darmstadt, Germany

three-dimensional (3D) first-mode disturbances prove to be significantly more unstable than the two-dimensional (2D) instabilities (Mack 1969, 1984). For boundary layers of higher Mach numbers, however, Mack found that in addition to the Tollmien-Schlichting-like waves, called first modes, further unstable modes appear, collectively known as Mack modes, which are high-frequency acoustic waves. Of particular importance is the Mack mode with the lowest frequency, the so-called second mode, as for high Mach numbers above approximately 4 the disturbances of the second mode grow faster than the first-mode instabilities. Unlike the first mode, the 2D perturbations of the second modes turn out to be the most unstable. Consequently, since in highly supersonic and hypersonic boundary layers the most unstable growth is determined by the 2D second-mode disturbances, investigations of factors that influence the stability of the second mode are of great importance.

Among other aspects, the surface temperature and its mechanical properties have a significant influence on the boundary layer stability. As Gaponov (1977) showed, porosity of the wall leads to destabilization of the first mode. At the same time, ultrasound-absorbing porous coatings stabilize the second-mode perturbations of hypersonic boundary layers, as predicted by the theoretical analysis by Fedorov et al. (2001) and confirmed experimentally and numerically by Fievet et al. (2020). Wall porosity thus constitutes a promising mechanism for second-mode damping. An opposite effect is observed with wall cooling, which leads to stabilization of the first mode, as already shown by Lees & Lin (1946) for the 2D and by Mack (1969, 1984) for the 3D perturbations, but leads to destabilization of the second and higher modes. Although many studies have addressed boundary layer stability with wall cooling, most of them have been limited to relatively moderate levels of wall cooling, that is, wall temperatures T_w greater than the free-flow temperature T_∞ . Bitter & Shepherd (2015) considered as a possible reason that most experiments operate at low stagnation temperature and hence low free-stream temperature T_∞ , making wall cooling below T_∞ difficult. However, the rarely studied case of highly cooled boundary layers with wall-to-free-stream ratios $T_w/T_\infty < 1$ is relevant for some real flight scenarios (Malik 2003) as well as in high-enthalpy test facilities, where very high free-stream temperatures at short test durations are achieved, leading to ratios $T_w/T_\infty = 0.1\text{--}0.3$ (Bitter & Shepherd 2015).

Against this background, this work considers a supersonic boundary layer flow over a straight highly cooled wall, with the aim of investigating the flow stability under the effect of wall linings characterized by their impedance. For this purpose, we apply temporal stability analyses utilizing both the inviscid and the viscous linear stability theory.

2. Temporal linear stability formulation

According to linear stability theory for compressible flows, the flow is considered to be slightly perturbed, meaning that the flow variables q are composed of a steady base flow value q_0 plus a small, unsteady perturbation q' , namely $q = q_0 + q'$. Applying this decomposition to the conservation equations for the flow, the compressible Navier-Stokes equations (NSEs), and subtracting the steady equations for the base flow yields the evolution equations for the disturbances. Due to the assumption that the disturbances are small, nonlinear terms of the disturbances can be neglected, thereby leading to linear disturbance equations, known as linear stability equations. By simplifying the stability equations for the case of an inviscid flow and a simplified mean velocity and temperature profile in the following, we are able to determine an analytical solution that allows us to

reduce the inviscid stability problem to an algebraic eigenvalue equation (Section 2.1). In contrast, investigations based on viscous stability equations are performed in Section 2.2, revealing the influence of viscosity in comparison to the inviscid results.

2.1. Inviscid consideration

Inviscid linear stability theory has already been applied by Lees & Lin (1946) and discussed by Mack (1969, 1984) as a useful method to investigate stability in high Mach number boundary layers. This is because, in compressible boundary layer flows of high Mach number, the unstable growth is dominated by the second mode, which has been found to be inviscid (Fedorov 2011). Therefore, studies based on the inviscid theory, where the linear stability equations are simplified by neglecting the viscous effects, can provide good insight into the instability processes of highly supersonic or hypersonic boundary layers (Mack 1984).

In these inviscid linear stability equations, we also neglect heat conduction effects, considering them to have no effect on the high-frequency acoustic Mack modes, as stated by Rienstra & Hirschberg (2021) in the context of acoustic waves. In addition, we assume a parallel shear base flow, $\mathbf{v}_0 = (u_0(y), 0, 0)^T$, of an ideal gas with constant pressure p_0 and with temperature and density gradients $T_0(y)$ and $\varrho_0(y)$ normal to the wall. For nondimensionalization, we use the free-flow velocity u_∞ , the base flow pressure p_0 , and the boundary layer thickness δ as characteristic quantities.

Following the standard procedure in linear stability analysis, we formulate a normal-mode approach for the perturbations. In view of the fact that for high Mach number boundary layers the most unstable perturbations are 2D waves of the second mode (Mack 1969, 1984), we consider only 2D perturbations at this point. Therefore, the normal-mode ansatz reads

$$q' = \hat{q}(y) e^{i(\alpha x - \omega t)}. \quad (2.1)$$

This approach is a Fourier decomposition of the perturbations with respect to the streamwise coordinate x and time t , giving the perturbation amplitude $\hat{q}(y)$ as Fourier transform depending on the wall-normal coordinate y only. α and ω represent the streamwise wavenumber and frequency of the disturbance. In the context of temporal stability analysis, we look at temporally growing perturbations, implying that $\omega = \omega_r + i\omega_i$ is complex with ω_i as the temporal growth rate for real wavenumbers α . Therefore, ω_i represents the key quantity for the temporal stability behavior.

An advantage of the normal-mode approach becomes apparent when inserting it into the stability equations, transforming this linear partial differential equation system into a system of linear ordinary differential equations (ODEs), which can be reduced further to a single second-order ODE for the pressure perturbation amplitude $\hat{p}(y)$, the so-called compressible Rayleigh equation (CRE) (Criminale et al. 2018)

$$\frac{d^2 \hat{p}}{dy^2} + \left(\frac{2\alpha}{\omega - \alpha u_0} \frac{du_0}{dy} + \frac{1}{T_0} \frac{dT_0}{dy} \right) \frac{d\hat{p}}{dy} + \left(\frac{M^2 (\omega - \alpha u_0)^2}{T_0} - \alpha^2 \right) \hat{p}(y) = 0, \quad (2.2)$$

where $M = u_\infty/a_\infty$ denotes the Mach number, with a_∞ as the far-field speed of sound.

For Eq. (2.2) to describe the boundary layer stability, $u_0(y)$ and $T_0(y)$ have to be chosen. For the velocity, we use an exponential profile, given in its nondimensionalized form by

$$u_0(y) = (1 - e^{-y}). \quad (2.3)$$

This turbulent boundary layer profile was derived by Oberlack (2001) and validated

numerically and experimentally for the mid-wake region of a high Reynolds number flat-plate boundary layer (Khujadze & Oberlack 2004; Lindgren et al. 2004). To model the temperature profile, we use the nondimensionalized quadratic Crocco-Busemann temperature-velocity relation

$$T_0(y) = \frac{T_w}{T_\infty} + \frac{T_{aw} - T_w}{T_\infty} u_0(y) + \frac{T_\infty - T_{aw}}{T_\infty} u_0(y)^2 \quad (2.4)$$

for non-isentropic zero-pressure-gradient boundary layer flows at Prandtl number $Pr = 1$ (Van Driest 1952). Here, T_w and T_∞ are the wall and free-stream temperature, while T_{aw} represents the wall temperature in the case of an insulated wall, the so-called adiabatic wall temperature. For $Pr = 1$, it is given by $T_{aw} = T_\infty(1 + (\kappa - 1)M^2/2)$, with κ as the specific heat capacity ratio, which we assume to be $\kappa_{air} = 1.4$. As further discussed in Section 3, we simplify the temperature profile to

$$T_0(y) = \frac{T_w}{T_\infty} \left(1 - \tilde{T} u_0(y)\right)^2, \quad (2.5)$$

with \tilde{T} defined by the temperature ratio $(1 - \tilde{T})^2 = T_\infty / T_w$. This allows us to derive an exact solution for the CRE (Eq. (2.2)) with the profiles in Eqs. (2.3) and (2.5) inserted: We find that the CRE with these profiles has four regular singularities at partly complex valued points $y_s = \{\infty, -\ln((\tilde{T} - 1)/\tilde{T}), -\ln(1 - \omega/\alpha), \infty + ik\pi\}$. The integer k depends on the choice of the natural logarithm's branch cut. According to Ronveaux (1995), any ODE with four regular singularities can be transformed into the general Heun equation (GHE)

$$\frac{d^2 w}{dz^2} + \left(\frac{\gamma}{z} + \frac{\delta}{z-1} + \frac{\epsilon}{z-a}\right) \frac{dw}{dz} + \frac{\alpha^* \beta z - q}{z(z-1)(z-a)} w = 0, \quad (2.6)$$

including five parameters and four regular singularities at $z_s = \{0, 1, a, \infty\}$. In order to transform the CRE into the GHE, first the transformation

$$z = \frac{\tilde{T}}{\tilde{T} - 1} e^{-y} \quad (2.7)$$

is applied on the independent variable to map three of the singularities of the CRE to the three singularities 0, 1 and ∞ of the GHE. A fourth singularity is brought to $a = \tilde{T}(\alpha - \omega)/(\alpha(\tilde{T} - 1))$, the so-called critical layer. Second, we carry out a transformation of the dependent variable reading

$$\hat{p}(z) = w(z) \cdot z^{r_1} (z-1)^{r_2} (z-a)^{r_3}, \quad (2.8)$$

where r_j are the roots of the Frobenius series expansions at the singularities 0, 1 and a (Ronveaux 1995). By this transformation, the CRE is converted into the form of Eq. (2.6), which gives the parameters of the GHE as functions of $M, \tilde{T}, \alpha, \omega$. The solution of the problem is thus given in terms of the general Heun function (Ronveaux 1995)

$$w(z) = C_1 \cdot \text{HeunG}(a, q; \alpha^*, \beta, \gamma, \delta, z) + C_2 \cdot z^{1-\gamma} \text{HeunG}(a, q_1; \alpha_1^*, \beta_1, \gamma_1, \delta, z). \quad (2.9)$$

Transforming Eq. (2.9) according to Eq. (2.8) yields the solution $\hat{p}(y)$ of the CRE.

In order to describe the stability problem completely, boundary conditions are required. As is common in stability theory, the perturbations are requested to vanish in the far field, giving the condition $\hat{p}(y \rightarrow \infty) = 0$. As can be derived using $\text{HeunG}(\cdot, z)|_{z=0} = 1$, the CRE solution $\hat{p}(y)$ can satisfy the far-field condition only if $C_1 = 0$. To model the behavior at the non-rigid wall, we introduce the wall impedance Z , which couples the

pressure fluctuation and the wall-normal velocity fluctuation in the frequency domain, namely $\hat{p}(\mathbf{x}, \omega) = Z(\mathbf{x}, \omega) (\hat{\mathbf{v}}(\mathbf{x}, \omega) \cdot \mathbf{n}(\mathbf{x}))$ (Rienstra & Hirschberg 2021). Based on this definition of the wall impedance, we can derive a wall boundary condition for the pressure perturbation amplitude \hat{p} by using the Fourier-transformed inviscid linear stability equations to express the velocity perturbation amplitude \hat{v} by the pressure perturbation amplitude's gradient, yielding the boundary condition

$$\hat{p}(y=0) = Z(\omega) \frac{i}{(1 - \tilde{T})^2 M^2 \omega} \frac{d\hat{p}}{dy} \Big|_{y=0} \quad (2.10)$$

for a straight wall with an impedance Z independent of the surface position \mathbf{x} . By inserting the solution $\hat{p}(y)$ of the CRE, with $C_1 = 0$ due to the far-field condition, into Eq. (2.10), the boundary value problem is transformed into an algebraic equation. It forms an algebraic eigenvalue problem for the complex eigenvalues $\omega(\alpha; M, \tilde{T}, Z)$ and thus constitutes the key equation for the inviscid temporal stability investigation, allowing the temporal growth rate ω_i of the eigenvalues to be examined for changes in the parameters.

The algebraic eigenvalue equation is solved regarding the change of both the real and imaginary parts of its residual. If both change their sign at the same value ω , the eigenvalue equation has a zero and, thus, the respective value is an eigenvalue. For the evaluation of the general Heun functions, we use their implementation in MATLAB by Motiygin (2015).

2.2. Viscous consideration

In contrast to the inviscid approach in the previous section, we want to take into account viscous effects in this section. As viscous model we use the full nondimensionalized linearized compressible Navier-Stokes equations (NSE) for an ideal gas with a temperature dependent viscosity governed by Sutherland's law (Malik 1990). As base flow, we apply the exponential velocity profile (2.3) and the (simplified) Crocco-Busemann temperature relation (2.5). Applying the normal mode approach in the linearized NSE yields

$$\mathbf{L}\mathbf{q} = \omega\mathbf{I}\mathbf{M}\mathbf{q}, \quad (2.11)$$

where \mathbf{q} is the vector of the perturbation amplitudes $\mathbf{q} = (\hat{u}(y), \hat{v}(y), \hat{\rho}(y), \hat{T}(y))^T$. The matrices \mathbf{L} , \mathbf{I} , \mathbf{M} can be found in Malik (1990). To enable comparison with the inviscid solution \hat{p} , the pressure perturbation is obtained by the linearized nondimensionalized ideal gas law $\hat{p} = T_0 \hat{\rho} + \hat{T}/T_0$.

Regarding the boundary conditions we assume, consistent with the inviscid consideration, vanishing perturbations in the freestream. At the wall, in addition to the impedance boundary condition discussed in Section 2.1, more boundary conditions are required for the viscous equations since they have higher order than the inviscid ones. Following Criminale et al. (2018), we assume a high thermal mass of the cooled or heated wall, which justifies vanishings temperature fluctuations at the wall, i.e. $\hat{T}(y=0) = 0$. Further we use a no-slip wall boundary condition, implying $\hat{u}(y=0) = 0$ for the horizontal velocity perturbation.

The differential eigenvalue problem, formed by Eq. (2.11) and the boundary conditions, is discretized using the Chebyshev spectral collocation method as described by Malik (2006). The equations are evaluated at the Gauss-Lobatto collocation points

$$\xi_j = \cos\left(\frac{j\pi}{N}\right), \quad j = 0, 1 \dots N, \quad (2.12)$$

which are the extrema of the Chebyshev polynomial T_N of N -th order. A stretched map for the Gauss-Lobatto points in the coordinate ζ , where half of the collocation points are located under a certain y value, y_h , allows us to resolve the wall-near area more precisely, as it is relevant due to steep gradients of the base flow in the near-wall region. The physical domain $y \in [0, \infty[$ is first mapped to the Chebyshev domain $\xi \in [-1, 1]$, which is then mapped to the stretched domain in the variable ζ by the transformation

$$\zeta_j = \frac{y_h y_{max} (1 + \xi_j)}{y_{max} - \xi_j (y_{max} - 2y_h)}, \quad (2.13)$$

as used by others such as Schmid & Henningson (2001). For the computational process, we restrict the maximum value of y to $y_{max} = 100$. The eigenfunctions $\mathbf{q}(\zeta_j)$ are expressed as linear combination of the Chebyshev polynomials. The boundary conditions are implemented as follows: We replace the continuity equation in the far field by the wall-normal momentum equation to apply an artificial condition on density, as used in Malik (2006). All boundary conditions are imposed weakly using an imposed spurious eigenvalue for the boundary modes. Finally, we obtain the discretized form of the eigenvalue problem (Eq. (2.11)), which is solved using the QZ algorithm implemented by MATLAB yielding its eigenvalues and eigenvectors.

3. Results

The main goal of this work is to investigate the effect of wall impedance on the temporal stability behavior of a high-velocity cooled boundary layer. In advance, we want to check whether the simplified Crocco-Busemann temperature-velocity relation, which we applied to derive the analytical inviscid solution, can provide good results. For this purpose, we first discuss the differences between the simplified and the full Crocco-Busemann relation. Second, we compare the eigenvalues of the inviscid solution with those obtained by the viscous solver. Third, we investigate the combined influence of wall impedance and wall cooling on the eigenvalues. All results discussed below are determined exemplary for $\alpha = 1.1$, $M = 4.2$ and $T_\infty = 1$.

To compare the simplified and the non-simplified Crocco-Busemann profiles, Figure 1 presents both profiles for different wall temperature cases: a strongly cooled wall, an insulated wall where the wall temperature equals the adiabatic wall temperature T_{aw} , and a heated wall. As shown in the figure, in case of the heated wall, the difference between the profiles is smaller than in the cooled wall case, where the simplified profile does not replicate the inflection point. It is therefore necessary to ascertain whether results based on the simplified temperature profile are nevertheless suitable for the planned stability investigation of a strongly cooled boundary layer. For this purpose, we compare for several strong wall cooling conditions the two rigid wall eigenvalue spectra at $Re = 20000$ obtained by the viscous solver for the full temperature relation on the one hand and for the simplified relation on the other hand. At $T_w/T_\infty = 2/3$, we find for the full profile the most unstable second mode at $\omega = 0.9912 + 0.0016i$, for the simplified one at $\omega = 0.862019 + 0.009382i$. The same trend is observed for other wall cooling configurations: The simplified profile leads to a more unstable second mode with lower phase velocity than the full profile. Summing up, the simplified temperature relation yields a more conservative prediction of the second mode's temporal growth rate. Therefore, for the following stability investigation, we consider both the inviscid and the viscous solution, using the simplified profile also for the viscous solver for the sake of comparability. If not stated otherwise, all results are obtained for the cooling $T_w/T_\infty = 2/3$.

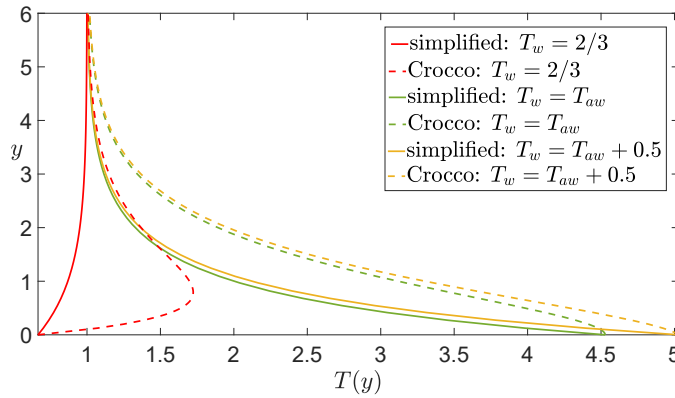


FIGURE 1. Simplified and full Crocco-Busemann temperature profiles for different wall temperature conditions at $T_\infty = 1$.

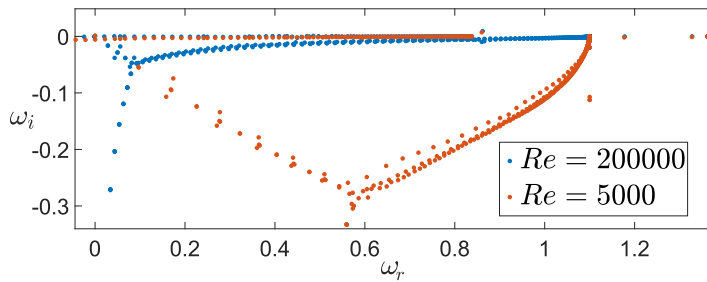


FIGURE 2. Viscous eigenvalue spectrum for two different Reynolds numbers.

In order to compare the inviscid and viscous eigenvalue spectra, we aim to identify in advance the eigenvalues of the viscous spectrum that are purely viscous, not being obtained from the inviscid solution. For this purpose, we examine how the eigenvalues of the viscous spectrum change as the Reynolds number is increased, nearing the inviscid limit $Re \rightarrow \infty$. As shown in Figure 2 for $Re = 5000$ and $Re = 200000$ in comparison, one eigenvalue branch turns up to the neutrally stable axis ($\omega_i = 0$) with increasing Reynolds number, leading us to interpret this branch as purely viscous. In comparison, especially the most unstable eigenvalue at $\omega \approx 0.86 + 0.008i$ seems almost unaffected by the Reynolds number and thus is expected to occur also in the inviscid case.

In the next step, we compare the viscous eigenvalue spectrum computed at $Re = 200000$ with the eigenvalues found by solving the inviscid eigenvalue problem, for both the case of a rigid wall and the case of an impedance wall with $Z = 140$ (Figure 3). For the rigid wall case, the most unstable mode of the viscous spectrum (blue circles) and the inviscid spectrum (red crosses) is found in the region of $\omega_r \approx 0.9$ with growth rate $\omega_i \approx 0.01$, as marked in Figure 3 by box (a). Here, the inviscid eigenvalue shows a slightly higher phase velocity ω_r/α and occurs with a stable complex-conjugate counterpart. Plots of the eigenfunctions of the most unstable eigenvalue show one zero crossing for both solutions, revealing that it is a second-mode perturbation. This is consistent with the literature stating that for high Mach numbers the second mode becomes dominant.

Regarding neutral modes, Figure 3 shows that the inviscid solution provides several

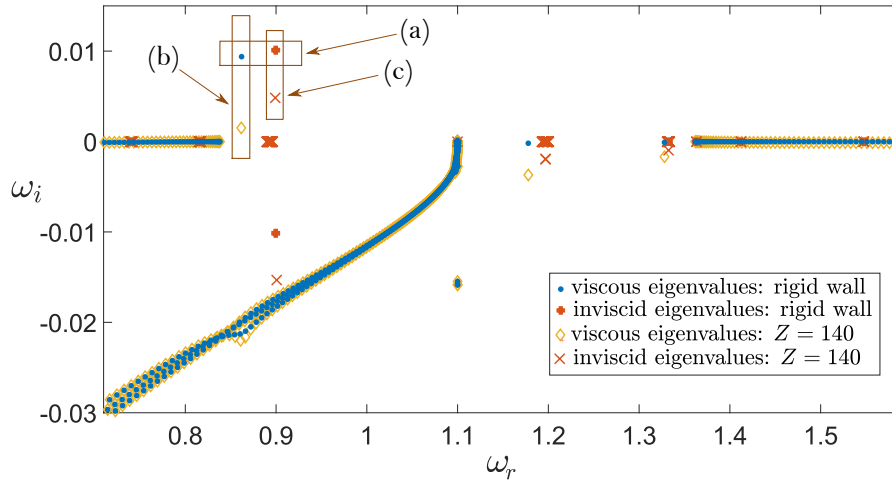


FIGURE 3. Viscous and inviscid eigenvalue spectra for both a rigid wall and an impedance wall with $Z = 140$.

discrete neutral stable eigenvalues. In particular, we find a neutrally stable inviscid eigenvalue that coincides with the beginning of the eigenvalue branch that was identified previously as purely viscous. A further neutrally stable inviscid eigenvalue fits with the beginning of a neutrally stable viscous eigenvalue branch originating at $\omega_r \approx 1.36$. Additionally, we want to point out that for every discrete neutrally stable viscous eigenvalue we find an inviscid counterpart.

Given the aim of the work to study the influence of wall impedance on the boundary layer stability, we now compare the viscous and inviscid eigenvalue spectra for the rigid wall case with the viscous and inviscid spectra obtained for an impedance wall. In this context, the difference in the growth rate of the most unstable second-mode disturbance is especially important. As shown in Figure 3, introducing the impedance wall with $Z = 140$ provides a reduction in the growth rate of the most unstable mode, implying that the impedance enables damping of the unstable growth as intended. Here, the viscous model predicts a stronger damping effect than the inviscid model; see Figure 3, boxes (b) and (c). In addition, the second-mode instability of the inviscid solution no longer appears complex-conjugate, since the imaginary part of the initial complex-conjugate stable eigenvalue is also reduced by the impedance. Further, we find that some of the discrete neutral modes beyond the viscous continuous branch are also stabilized, whereas the purely viscous eigenvalue branch as well as the continuous neutrally stable branches seem to be unaffected by the impedance.

Because the stabilization of the most unstable perturbation is especially important, we finally in Figure 4 in more detail the evolution of the second-mode growth rate under impedance variation using both the inviscid (a) and viscous (b) solutions. Therefore, an infinite wall impedance corresponds to the rigid wall case. The growth rate as a function of the impedance is presented for different wall temperatures. It is found that increasing the wall cooling, namely a smaller T_w/T_∞ ratio, leads to destabilization. This destabilizing effect due to stronger cooling is more prominent in the inviscid model than in the viscous one. Regardless of the temperature ratio T_w/T_∞ , however, both models equally predict damping of the unstable second-mode growth for sufficiently small wall impedances.

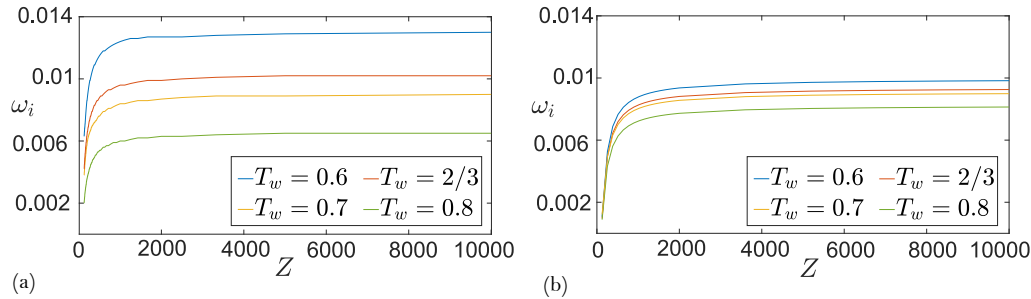


FIGURE 4. Influence of wall impedance and temperature on the second mode for (a) the inviscid and (b) the viscous case at $Re = 200000$.

4. Conclusions

In this work, we investigated the eigenmodes of the temporal stability problem for a compressible high-velocity boundary layer flow over a highly cooled impedance wall. We gave an inviscid as well as a viscous treatment of the problem and compared both results. The inviscid solution of the eigenvalue problem, based on a newly found exact solution of the linearized perturbed equations, showed good agreement with the viscous Chebyshev collocation solution with regard to the dominant unstable mode and discrete neutral modes.

One main goal of this work was to quantify the influence of non-rigid impedance walls. Both models showed the same behavior; the impedance wall clearly stabilizes the discrete eigenvalues, where the viscous model predicts a stronger damping effect than the inviscid one. Since the transition to turbulence is affected not only by the long-term behavior of the perturbations but also by short-term mechanisms such as the well-known transient growth mechanism, we aim to use the completely calculated spectrum in future work to evaluate the damping effect of impedance on short-term growth. It is also conceivable for further work to implement an extension of the existing impedance model, which takes into account the frequency dependence of wall impedance reminiscent of engineered surfaces such as porous surfaces.

This work thus provides the basis to study the transition process based on temporally evolving instabilities for the flow type considered and to define measures to delay the transition.

Acknowledgments

The authors are very grateful to Prof. Peter Schmid and Dr. Olaf Marxen for extremely helpful discussions on the numerical treatment of stability problems, transient growth, and the evolution of spatially growing disturbances.

REFERENCES

- BITTER, N. P. & SHEPHERD, J. E. 2015 Stability of highly cooled hypervelocity boundary layers. *J. Fluid Mech.* **778**, 586–620.
- CRIMINALE, W. O., JACKSON, T. L. & JOSLIN, R. D. 2018 *Theory and Computation in Hydrodynamic Stability*. Cambridge University Press.
- DUNN, D. W. & LINN, C. C. 1955 On the Stability of the Laminar Boundary Layer in a Compressible Fluid. *J. Aeronaut. Sc.* **22**, 455–477.
- FEDOROV, A. 2011 Transition and stability of high-speed boundary layers. *Annu. Rev. Fluid Mech.* **43**, 79–95.
- FEDOROV, A. V., MALMUTH, N. D., RASHEED, A. & HORNUNG, H. G. 2001 Stabilization of hypersonic boundary layers by porous coatings. *AIAA J.* **39**, 605–610.
- FIEVET, R., DENIAU, H., BRAZIER, J.-P. & PIOT, E. 2020 Numerical study of hypersonic boundary-layer transition delay through second-mode absorption. *AIAA Paper 2020-2061*.
- GAPONOV, S. A. 1977 Stability of a supersonic boundary layer on a permeable surface with heat transfer. *Fluid Dyn.* **12**, 33–38.
- KHUJADZE, G. & OBERLACK, M. 2004 DNS and scaling laws from new symmetry groups of ZPG turbulent boundary layer flow. *Theor. Comp. Fluid Dyn.* **18**, 391–411.
- LEES, L. & LINN, C. C. 1946 Investigation of the stability of the laminar boundary layer in a compressible fluid. *NACA Tech. Note 1115*.
- LINDGREN, B., ÖSTERLUND, J. M. & JOHANSSON, A. 2004 Evaluation of scaling laws derived from Lie group symmetry methods in zero-pressure-gradient turbulent boundary layers. *J. Fluid Mech.* **502**, 127–152.
- LYSENKO, V. I. & MASLOV, A. A. 1984 The effect of cooling on supersonic boundary-layer stability. *J. Fluid Mech.* **147**, 39–52.
- MACK, L. M. 1969 Boundary layer stability theory. *JPL Report 900-277*. Jet Propulsion Lab, California Institute of Technology.
- MACK, L. M. 1984 Boundary layer stability theory. *AGARD Report 709*. North Atlantic Treaty Organization.
- MALIK, M. R. 1990 Numerical methods for hypersonic boundary layer stability. *J. Comput. Phys.* **86**, 376–413.
- MALIK, M. R. 2003 Hypersonic flight transition data analysis using parabolized stability equations with chemistry effects. *J. Spacecraft Rockets.* **40**, 332–334.
- MALIK, M. R. 2006 Nonmodal energy growth and optimal perturbations in compressible plane Couette flow. *Phys. Fluids* **18**, 034103.
- MOTYGIN, O. V. 2015 On numerical evaluation of the Heun functions. In *Days on Diffraction 2015*, pp. 1–6.
- OBERLACK, M. 2001 A unified approach for symmetries in plane parallel turbulent shear flows. *J. Fluid Mech.* **427**, 299–328.
- RIENSTRA, S. W. & HIRSCHBERG, A. 2021 *An Introduction to Acoustics*. Eindhoven University of Technology.
- RONVEAUX, A. 1995 *Heuns differential equations*. Oxford University Press.
- VAN DRIEST, E. R. 1952 Investigation of laminar boundary layer in compressible fluids using the Crocco method. *NACA Tech. Note 2597*.
- SCHMID, P.J. & HENNINGSON, D. 2001 *Stability and Transition in Shear Flows*. Springer.